Applied Physics Express



**LETTER** • **OPEN ACCESS**

# Classical SPICE simulation of superconducting quantum circuits

To cite this article: Tetsufumi Tanamoto *et al* 2023 *Appl. Phys. Express* **16** 034501

OPEN ACCESS

Applied Physics Express 16, 034501 (2023) LETTER

https://doi.org/10.35848/1882-0786/acc3d8

# Classical SPICE simulation of superconducting quantum circuits

Tetsufumi Tanamoto[1*], Toyofumi Ishikawa[2], Kunihiro Inomata[2], Shumpei Masuda[2], Tamio Omuma[1], and Shiro Kawabata[2]

[1]Department of Information and Electronic Engineering, Teikyo University, 1-1 Toyosatodai, Utsunomiya 320-8551, Japan
[2]Research Center for Emerging Computing Technologies (RCECT), National Institute of Advanced Industrial Science and Technology (AIST), Tsukuba, Ibaraki 305-8568, Japan

*E-mail: tanamoto@ics.teikyo-u.ac.jp

Received January 23, 2023; revised February 16, 2023; accepted March 12, 2023; published online March 31, 2023

Quantum computing has been developed for many physical systems, and superconducting qubits are now in the integration phase. To efficiently design a many qubit system, an appropriate circuit simulator is necessary. Despite the existence of simulators for circuits including Josephson junctions, simpler circuit simulators are desirable when considering integrated qubits controlled by millions of transistors. This study examines the application of conventional Simulation Program with Integrated Circuit Emphasis simulators to analyze transmission signals of the system composed of transmons in the dispersive regime. Further, the influences of device parameter variations caused by the fabrication process can be taken into the model. 

Quantum computing is a popular topic in physics and engineering. Many institutes and companies have competed in the development of small and intermediate scale quantum computers. Circuit quantum electrodynamics architecture is a promising platform for quantum computing, and the further integration of superconducting qubits is required for realizing universal quantum computers.[1–11] From the perspective of integration, the engineering of a circuit that includes qubits and other circuit elements such as amplifiers, filters, and mixers is a key factor.

Circuit simulators are crucial to the design of large integrated systems.[12] Unnecessary fabrication can be avoided by using circuit simulations and shortening the manufacturing period. In this phase, a Simulation Program with Integrated Circuit Emphasis (SPICE) simulator may be most suitable because of its wide popularity among complementary metal oxide semiconductor (CMOS) engineers. Josephson junctions do not exist in conventional CMOS SPICEs and thus far, various software such as WRSPICE,[13] PSCAN,[14] and JSIM[15] have been developed to simulate superconducting classical circuits with the Josephson junctions.

Currently, the number of qubits is of the order of several hundreds. They are controlled through several equipments that include millions of transistors.[16] For example, certain experiments[4] require arbitrary waveform generators, vector network analyzers, analog-to-digital (ADC) converters, and other electronic apparatus, and they are constructed using CMOS transistors. Ideal quantum circuits are integrated with classical CMOS circuits in a single chip to enhance the efficiency of quantum computers. Accordingly, a combination of superconducting quantum and classical circuits with conventional CMOS circuits require faster and lighter simulations of superconducting parts.

Rapid developments in transistors and CMOS circuits have frequently updated the SPICE software. Currently, various SPICE software packages are widely available with and without a fee. However, quickly updating the aforementioned specific SPICEs for superconducting quantum circuits is challenging. This is considered a serious issue when many CMOS engineers must join in building large-scale quantum computers. Thus, it is important to describe superconducting quantum circuits using classical CMOS circuits to ensure smooth preparation of peripheral circuits of qubits. With an increase in the number of qubits and circuit component complexity, succinct circuit simulations are required to reduce the calculation time. Consequently, the number of parameters that characterize the circuit components should be small. It is evident that classical circuits cannot perfectly reproduce quantum circuits. In particular, quantum gate operations cannot be described using classical circuits, and it is not straightforward to classically describe the amplifier using Josephson junctions. However, by focusing on the linear response regime of the linear-resonator circuit model, quantum circuits can be approximated by classical circuits. Many researchers have described quantum circuits using classical circuits to explain the simplest picture of superconducting circuits. In particular, the output process through the transmission lines is described using classical LC circuits.[2,7] Goppl et al.[7] experimentally investigated the relation between the classical LCR model and its device structure, and showed that the classical LCR model describes the experimental setup.

This study describes the measurement part of the circuits with superconducting qubits using a conventional SPICE simulator. In particular, the transmission measurement of superconducting circuits with resonators and Purcell filters[4] are examined using SPICE. Transmission measurements of superconducting circuits are widely used to extract system parameters. The linear response of the system under transmission measurement is focused upon, neglecting the quantum nature and nonlinearity of the qubits. The dispersive regime,[2,3] where the frequency of the readout resonator is far from the qubit frequency, is considered.

The circuit under analysis in this study comprises of a transmission line, LCR circuit element of qubits, and readout resonators. Here, the qubit is described by the longitudinal relaxation time $T_1^{(q)}$, with capacitance $C$ and resistance $R$ as the input parameters. The photons in the transmission line interact with the qubit regarding the energy difference $\omega_q$

between the ground and first excited states.[2] When the resonator frequency $\omega_r$ is far from $\omega_q$, the nondestructive readout is expected. The relaxation rate of the qubit decreases as the detuning, defined as $\Delta_{qr} \equiv \omega_r - \omega_q$, increases. The dissipation is assumed to be described by the resistance in the LCR circuits with the relationship $T_1^{(q)} = CR$.[5,8] Thus, the dissipation $R$ can be obtained using $T_1^{(q)}$ and $C$. From the relationship $\omega_q = 1/\sqrt{LC}$, inductance $L$ is calculated using $\omega_q$ and $C$. Consequently, three basic input parameters: $\omega_q$, $T_1^{(q)}$, and $C$ can be considered. The capacitances $C$ are of the order of 10 fF, and the frequencies $\omega_q/2\pi$ are of the order of GHz, Thus, $C\omega_q \sim 10\,\text{fF} \times \text{GHz} \sim 10^{-5}\ \ \Omega^{-1}$. Assuming $T_1^{(q)} = 1\ \mu\text{s}$, the resistance $R$ is expressed as: $1/R \sim C/T_1 \sim 10\,\text{fF}/1\ \mu\text{s} = 10^{-8}\ \ \Omega^{-1}$, and $1/R \ll C\omega_q$ are obtained. We assume that the qubit and resonators are capacitively coupled to the transmission line. Following Ref. 2, consider the case when the strength of the qubit-resonator coupling $g$ in the Jaynes–Cummings model is proportional to the coupling capacitance $C_g$ between the qubit and the readout resonator, which is expressed as $g = \frac{C_g}{C_\Sigma}\frac{e}{\hbar}\sqrt{\frac{\hbar\omega_r}{C}}$, with typical values of $\omega_r/2\pi = 5$ GHz and $C = 50$ fF. Thus, we have

$$\frac{g}{2\pi} \approx 0.785\frac{C_g}{C_\Sigma}\ \text{GHz}, \tag{1}$$

where $C_\Sigma$ denotes the total capacitance of the Josephson junctions ($C_g/C_\Sigma < 1$). Therefore, in the range of $\Delta_{qr}/2\pi > 1$ GHz, $g/\Delta_{qr} \ll 1$ is maintained.

The qubit relaxation rate $\gamma_q$ is generally expressed as Ref. 4

$$\gamma_q \propto (g/\Delta_{qr})^2. \tag{2}$$

Obtaining a similar equation will prove the applicability of classical circuits. This study numerically examines this relationship between $\gamma_q$ and $\Delta_{qr}$ in the classical circuit depicted in Fig. 1. To reduce the Purcell effect (qubit-resonator coupling induces spontaneous emission),[4,17] the second resonator is introduced into the qubit-resonator system as a Purcell filter shown in Fig. 1(c).

As the simplest approach, lumped circuits are considered. In the standard dispersive readout, the resonant frequency changes depending on the qubit states $|0\rangle$ and $|1\rangle$. However, in classical LCR circuits, the feature of qubit is represented only by $\omega_q$. This is a limitation of the classical descriptions. Subsequently, for more realistic applications, two parameter sets must be prepared corresponding to the two-qubit states, $|0\rangle$ and $|1\rangle$, and the circuit parameters should be adjusted after fixing the qubit states, depending on $|0\rangle$ or $|1\rangle$. In this study, only the relationship between $\omega_q$ and transmission circuit behavior is focused upon without identifying the qubit state. Moreover, the effects of the variations in the circuit components are estimated.

For classical LCR circuits, the output of the transmission signal tends to have a sharper peak structure for a better resonant transmission line. The peak structure is assumed to be characterized by the ratio of peak $\omega_p$ to the full-width $\delta\omega_p$ at the half maximum given by $Q_p \equiv \omega_p/\delta\omega_p$. Moreover, the lifetime $T_1^{(m)}$ of the qubit by measurement is assumed to be expressed by $Q_p = \omega_p T_1^{(m)}$. Then we might be able to express

$$T_1^{(m)} \equiv \frac{1}{\delta\omega_p}. \tag{3}$$

Thus, Eq. (2) is investigated by checking whether $T_1^{(m)} \propto (\Delta_{qr}/C_g)^2$ is satisfied. Here, the output of the transmission line is examined by both the voltage and magnitude of transmission signal $S_{21}$, where the corresponding relaxation times are represented by: $T_1^{(m)v}$ and $T_1^{(m)s}$, respectively. Hereafter, $\Delta_{qr}$ is calculated from the output peak positions of the qubit frequency $\omega_q^{(m)}/2\pi$ and the resonator frequency $\omega_r^{(m)}/2\pi$, given by $\Delta_{qr} = \omega_r^{(m)} - \omega_q^{(m)}$.

Figures 2(a) and 2(b) show schematics of a single qubit coupled to a readout resonator described by LTSpice,[18] and Fig. 2(c) shows an example of the simulation results for the transmission signal $S_{21}$. The number of photons in the readout resonator is estimated as $n = P/\kappa\hbar\omega_{cv}$, where $P$ is the input microwave power, $\kappa$ is the photon decay rate in the transmission line whose typical resonant frequency is $\omega_{cv}$. On the other hand, $P$ can be calculated using the input current $I$ and resistance $R_0$ given by $P = R_0 I^2$: When considering $R_0 = 50\ \Omega$ and the typical transmission line decay rate $\kappa/2\pi = 1$ MHz with $\omega_{cv}/2\pi = 3$ GHz ($Q = 3000$), we have $I = \sqrt{\hbar\omega_{cv}\kappa/R_0} \approx 0.08$ nA. In the following circuit calculations, this value is used as the source current. For Fig. 2(a) [Fig. 2(b)], two (three) groups of the transmission peaks corresponding to the peaks of $Z_q$ and $Z_r$ [and $Z_p$ in Fig. 2(b)) are obtained. The relaxation time $T_1^{(m)}$ by the measurement is estimated numerically from the calculated peaks of $Z_q$. In

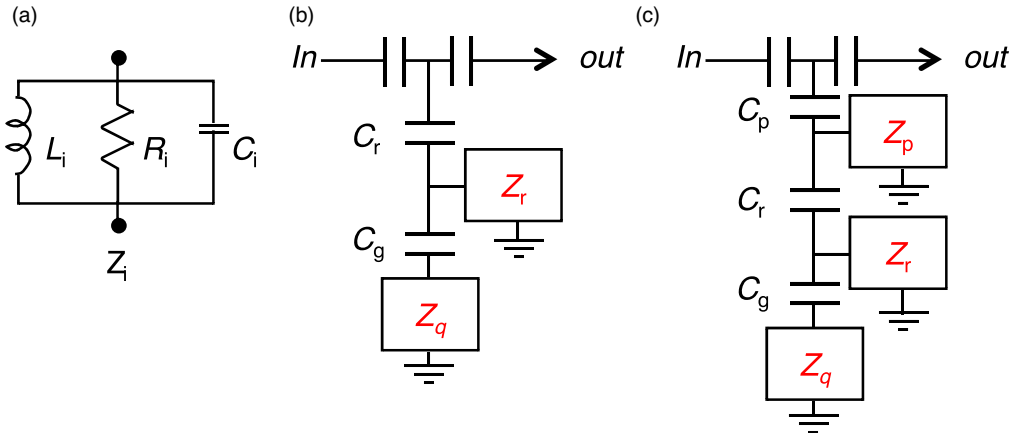


**Fig. 1.** (Color online) Circuit description in the dispersive regime. The qubit ($Z_q$) and readout resonators ($Z_r$ and $Z_p$) are approximated by LCR circuits (a) to be implemented into the SPICE circuit simulation. (b) The qubit and readout resonator. (c) The qubit with the tank and Purcell circuits ($Z_p$).

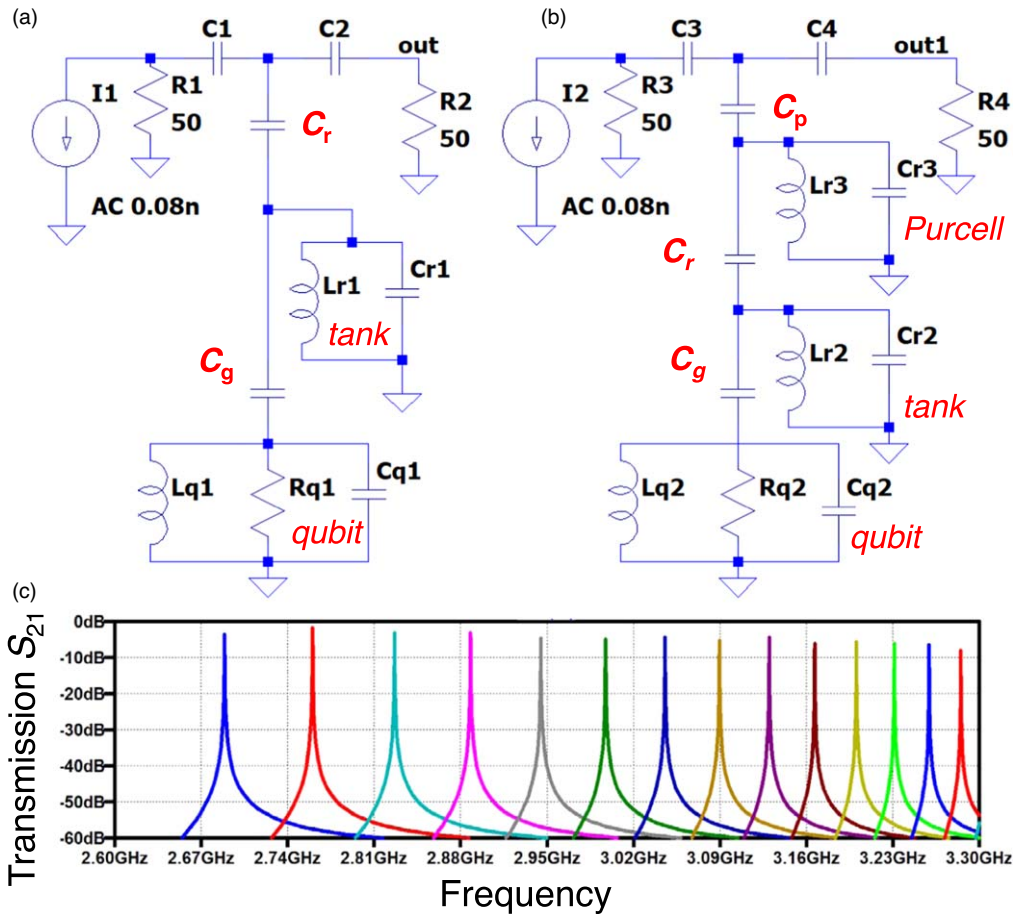


**Fig. 2.** (Color online) LTSpice schematics of the transmission line composed of the qubit (the lowest LCR circuit), and the readout resonators (upper LC circuits). (a) A qubit coupled to a readout resonator. (b) A qubit coupled to tank and Purcell circuits. (c) An example of the LTSpice simulation of the qubit characteristics of (a) when the resonator frequency $\omega_r/2\pi$ changes from 6 to 11 GHz with 250 MHz steps. The input qubit frequency is given by $\omega_q/2\pi = 6$ GHz, and all capacitances other than qubits are 50 fF. $C_{q1} = C_{q2} = 30$ fF. $T_1^{(q)} = 1$ $\mu$s.

addition, the output can be described by both the voltage and $S_{21}$. The corresponding $T_1^{(m)}$s are represented by $T_1^{(m)v}$ and $T_1^{(m)s}$, respectively, in the following calculations.

Figures 3(a) and 3(c) show the calculated $T_1^{(m)v}$ and $T_1^{(m)s}$ as a function of detuning $\Delta_{qr}$ for both $\Delta_{qr} > 0$ and $\Delta_{qr} < 0$. $T_1^{(m)s}$ has sharper peaks than $T_1^{(m)v}$. As evident, $T_1^{(m)v}$ and $T_1^{(m)s}$ increase with an increase in $|\Delta_{qr}|$. This result corresponds to that of the experiments conducted by Houck et al.[8] Regarding the relationship between $C_g$, $T_1^{(m)}$, both $T_1^{(m)v}$ and $T_1^{(m)s}$ increases for a larger $C_g$ in $\Delta_{qr} < 0$, whereas the relative magnitudes are exchanged for larger $\Delta_{qr}$. Thus, in a classical circuit model, it can be observed that the lifetime of the qubit increases with an increase in the detuning, although the coupling dependence is weaker than in the experiments. Moreover, when $T_1^{(m)v}$ of $C_g = 50$ fF ($C_g = 30$ fF) is extrapolated using polynomials, $T_1^{(m)v}[s] \approx 0.09\Delta_{qr}^2 - 0.08\Delta_{qr} - 0.07$ ($T_1^{(m)v}[s] \approx 0.05\Delta_{qr}^2 + 0.08\Delta_{qr} - 0.02$) is obtained as the function $\Delta_{qr}/2\pi$[GHz]. Thus, the coefficients of $\Delta_{qr}^2$ are slightly larger than those of other terms. Discrepancy from the experiments becomes prominent for larger detuning region, in which the interference between the qubit and resonator circuits become weak. Because our description is simple, the $T_1^{(m)s}$ based on the scattering matrix is less suitable to describe the experiments. The details should be investigated in the future.

The readout resonator enhances the relaxation of the qubits, referred to as the Purcell effect. The change in the relaxation owing to the second readout resonator is numerically investigated. Figures 3(b) and 3(d) show the comparison of $T_1^{(m)}$ values for Fig. 2(b) to confirm the effects of the Purcell filter. As evident, the second readout resonator (Purcell filter) increases the relaxation time as expected. However, $T_1^{(m)s}$ decreases with an increase in $\Delta_{qr}$. Thus, to estimate the relaxation time, $T_1^{(m)v}$ appears to be better.

When the number of qubits is increased, the fabrication of each component may not be precisely controlled, and the variations become a serious problem. One of the advantages of using simulations is that we can estimate the effects of variations in circuit components. Figure 4 presents the simulation results when $C_g$ is randomly distributed with a uniform 10% around the center value 40 fF. A variation in the frequency of $S_{21}$ is observed, which is expected to be measured as the transmission line output.

For example, the crosstalk problem could be significant as described in Ref. 6. Let us examine a case where the coupling capacitance $C_g$ between the qubit and readout resonator changes from the designed values because of variations. Figure 5(a) shows a sample schematics for eight qubits to observe the effect of the variations in many qubit systems. When $C_g$s vary uniformly by 5% at approximately $C_g = 40$ fF over 100 samples, the $S_{21}$ of the qubit part varies as shown in Fig. 5(b). Realistically, other parameters also vary, and this is an example that even the variation of a single parameter changes the performance. This kind of variations should be absorbed by the later-stage circuits. As mentioned above, as

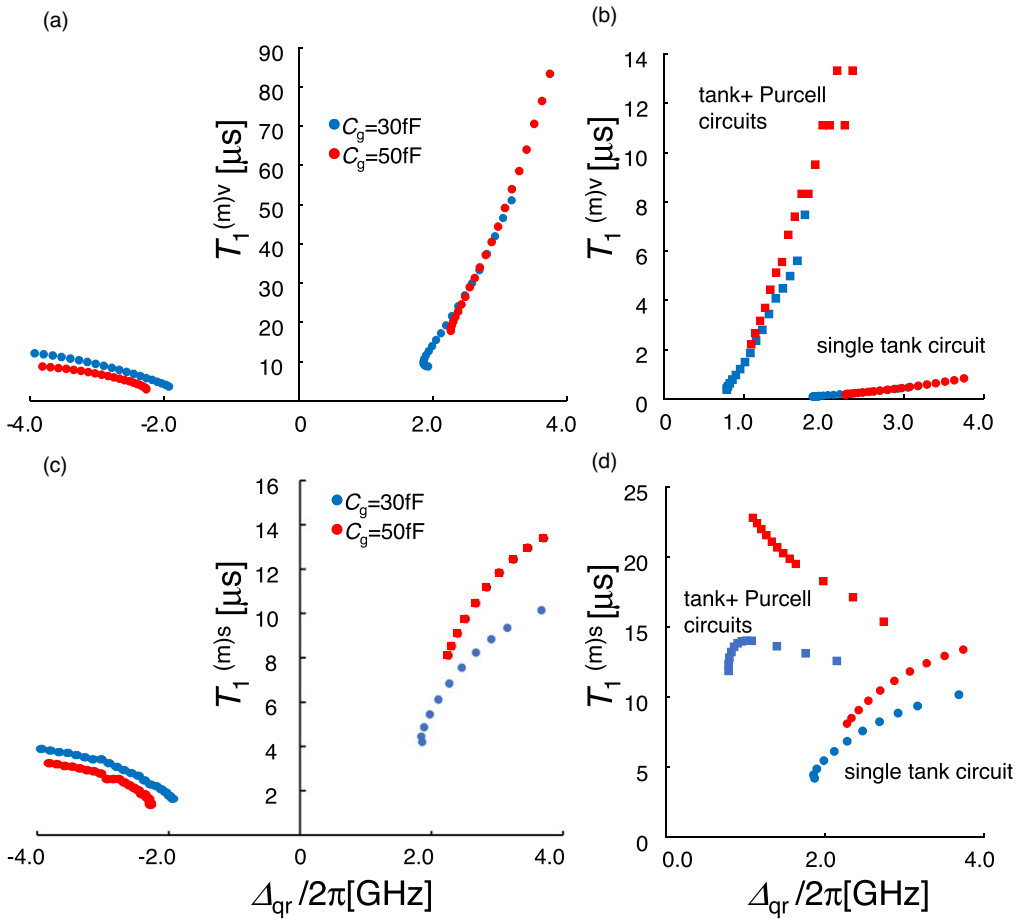


**Fig. 3.** (Color online) Relaxation times $T_1^{(m)v}$((a) and (b)) and $T_1^{(m)s}$((c) and (d)) calculated numerically based on LTSpice. Figs. (a) and (c) are the results of the circuit in Fig. 2(a), Figs. (b) and (d) are those in Fig. 2(b) as the function of the detuning $\Delta_{qr} \equiv \omega_r^{(m)} - \omega_q^{(m)}$. In Figs. (b) and (d), the tank and the Purcell circuits have the same parameters of $L$ and $C$ for simplicity. In the lefthand of Figs. (a) and (c), $\omega_r/2\pi$ changes from 1 to 6 GHz. The input qubit frequency is given by $\omega_q/2\pi = 6$ GHz.

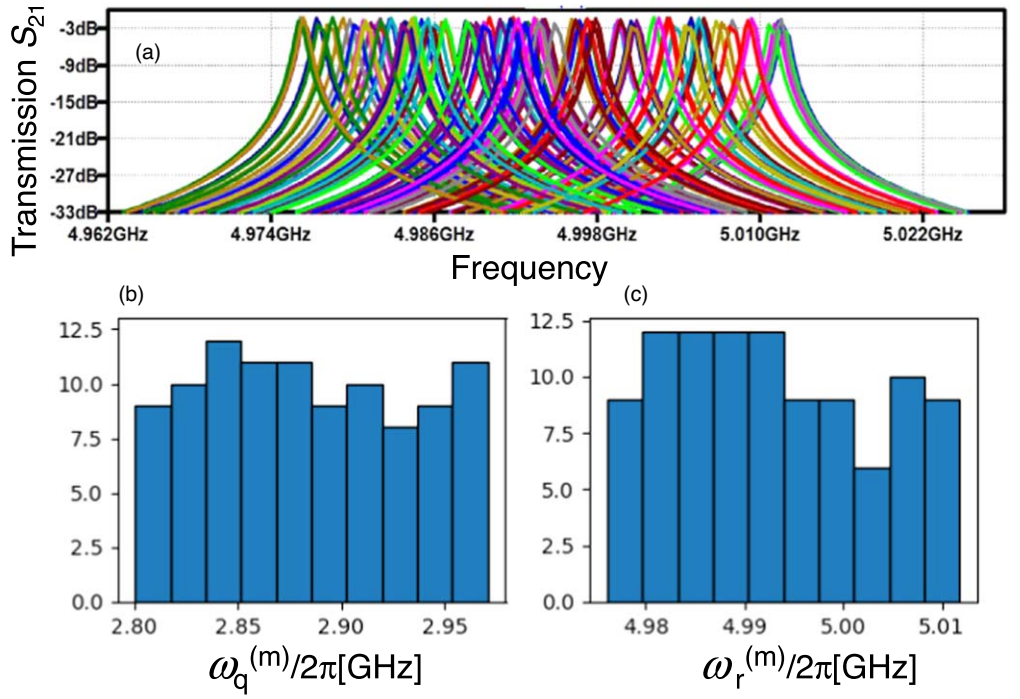


**Fig. 4.** (Color online) Monte Carlo simulation of the qubit-readout resonator described in Fig. 2(a). (a) Variation of $S_{21}$ over 100 samplings where $C_q$ is randomly distributed around uniform 10% with the center value 40 fF. (b) The histogram of the distribution of the qubit frequency $\omega_q^{(m)}/2\pi$ and (c) that of the resonator frequency $\omega_r^{(m)}/2\pi$, both of which are calculated from the positions of the output peaks.

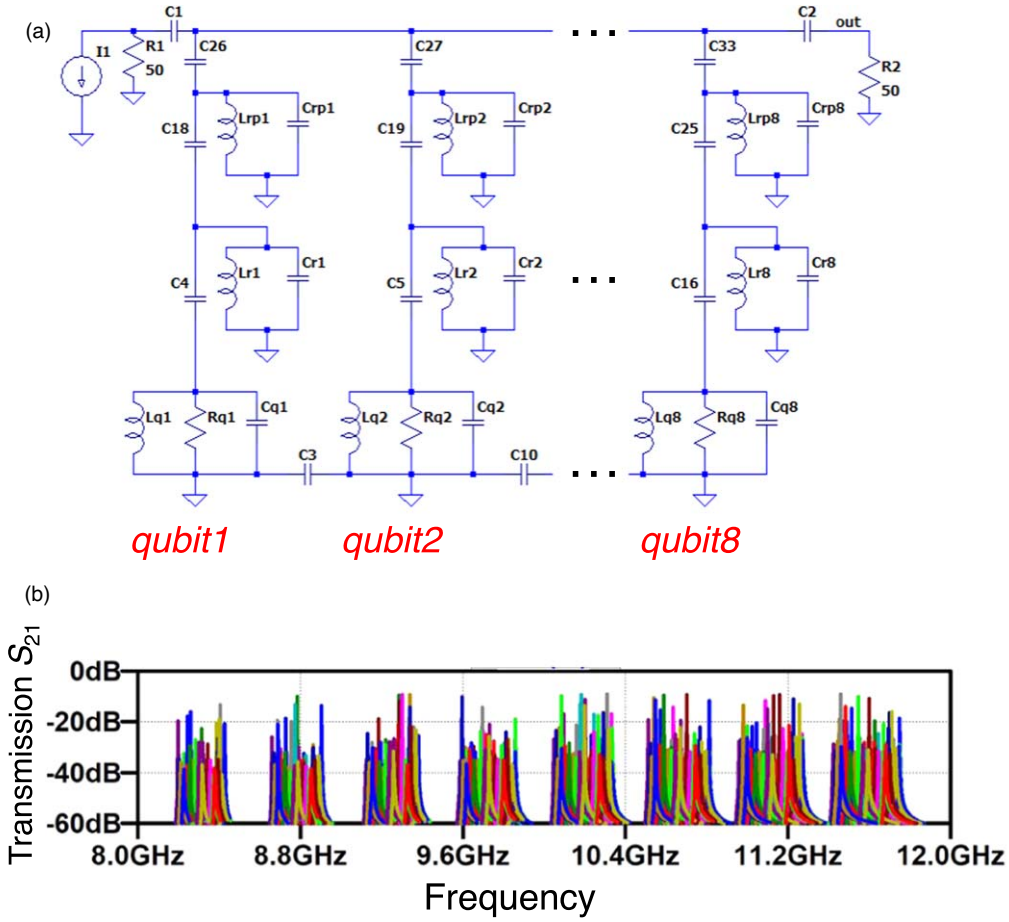


**Fig. 5.** (Color online) (a) The eight-qubit circuit. Capacitances noted by $C_x$ ($x$ are numbers) are on the order of 40–50 fF. Other parameters are the same as those in Fig. 2. (b) An example of Monte Carlo simulations for $S_{21}$ of the eight-qubit circuit. The 5% variations of $C_g$ cause the variations of the outputs $S_{21}$. The variations of parameter should be taken into account when designing large circuits.

one of the convenient uses of circuit simulations, the effects of variations in circuit parameters can be inferred. It is expected that the simple circuit simulator described here aids the design of later-stage circuits via the estimation of the operation margins.

In conclusion, this study proposed a classical circuit description for transmons in the dispersive regime. It is shown that a classical circuit can reproduce the basic relationship between relaxation time and detuning. Consequently, certain aspects of quantum circuits can be described using classical circuits. Thus, it is believed that classical simple circuits can aid in the design of many qubit systems. This study is focused on a lumped element circuit. In the near future, a corresponding model based on distributed element circuits including the amplifier and the mixers should be investigated and developed.

**Acknowledgments** We are grateful for the discussions with T. Mori and H. Fuketa. This study is partly based on the results obtained from the project JPNP16007, commissioned by the New Energy and Industrial Technology Development Organization (NEDO), Japan. This work was also partly supported by MEXT Quantum Leap Flagship Program (MEXT Q-LEAP), Grant Number JPMXS0118069228, Japan.

**ORCID iDs** Tetsufumi Tanamoto https://orcid.org/0000-0002-1373-2812 Toyofumi Ishikawa https://orcid.org/0000-0001-9089-0024

1) A. Wallraff, D. I. Schuster, A. Blais, L. Frunzio, R.-S. Huang, J. Majer, S. Kumar, S. M. Girvin, and R. J. Schoelkopf, Nature **431**, 162 (2004).
2) A. Blais, R.-S. Huang, A. Wallraff, S. M. Girvin, and R. J. Schoelkopf, Phys. Rev. A **69**, 062320 (2004).
3) J. Koch, T. M. Yu, J. Gambetta, A. A. Houck, D. I. Schuster, J. Majer, A. Blais, M. H. Devoret, S. M. Girvin, and R. J. Schoelkopf, Phys. Rev. A **76**, 042319 (2007).
4) P. Krantz, M. Kjaergaard, F. Yan, T. P. Orlando, S. Gustavsson, and W. D. Olive, Appl. Phys. Rev. **6**, 021318 (2019).
5) E. Jeffrey et al., Phys. Rev. Lett. **112**, 190504 (2014).
6) J. Heinsoo et al., Phys. Rev. Appl. **10**, 034040 (2018).
7) M. Göppl, A. Fragner, M. Baur, R. Bianchetti, S. Filipp, J. M. Fink, P. J. Leek, G. Puebla, L. Steffen, and A. Wallraff, J. Appl. Phys. **104**, 113904 (2008).
8) A. A. Houck et al., Phys. Rev. Lett. **101**, 080502 (2008).
9) D. Risté, M. Dukalski, C. A. Watson, G. de Lange, M. J. Tiggelman, Y. M. Blanter, K. W. Lehnert, R. N. Schouten, and L. DiCarlo, Nature **502**, 350 (2013).
10) Y. Sunada, S. Kono, J. Ilves, S. Tamate, T. Sugiyama, Y. Tabuchi, and Y. Nakamura, Phys. Rev. Appl. **17**, 044016 (2022).
11) S. Kwon, A. Tomonaga, G. L. Bhai1, S. J. Devitt, and J.-S. Tsai, J. Appl. Phys. **129**, 041102 (2021).
12) N. Materise, Springer Proc. Phys. **211**, 87 (2018).
13) S. R. Whiteley, IEEE Trans. Magn. **27**, 2902 (1991).
14) S. V. Polonsky, Supercond. Sci. Technol. **4**, 667 (1991).
15) E. S. Fang and T. van Duzer, IEEE Trans. Appl. Supercond. **1**, 126 (1991).
16) J. S. Park et al., 2021 IEEE Int. Solid-State Circuits Conference (ISSCC) Dig. Tech. Papers, 2021, p. 208.
17) E. A. Sete, J. M. Martinis, and A. N. Korotkov, Phys. Rev. A **92**, 012325 (2015).
18) Analog Devices SPICE Model Library (https://www.analog.com/en/design-center/design-tools-and-calculators/ltspice-simulator.html).